River delta eco-morphodynamics under changing scenarios. The case of Lake Turkana, Kenya

Simone Zen[1], **Paolo Perona**[1,2], **Encarni Medina-Lopez**[1]

[1]School of Engineering, Institute for Infrastructure and Environment, The University of Edinburgh, UK
[2]École Polytechnique Fédérale de Lausanne, Switzerland

Key Points:

- This paper analyses the impact of local climate, river hydrology, and the construction of three dams on river delta morphodynamics.
- Satellite imagery allowed us to quantify changes in land use and river morphology, and relate these to climate change and river hydrology.
- The dams diminished the amount of bare sediments, increased the density of biomass and low flow, and reduced the peak during flood season.

Corresponding author: E. Medina-Lopez, `emedina@ed.ac.uk`

Abstract

In this work we explore the impact that changes in local climate and river hydrology have on the morphodynamics of a river delta, particularly focusing on the evolution of the delta generating at the lake inlet. We investigated the case of the delta in the lower reach of the Omo River in Ethiopia, which flows into Lake Turkana, Kenya. The lake is the fourth largest lake and the largest desert lake in the world. This case study is of particular interest because within the last decades three dams have been built within the Omo basin. Among these, the Gibe III dam had a huge impact on the river hydrology and the sediment supply. To quantify changes in land use and river morphology and relate these to climate change and river hydrology we collect a historical dataset by combining information from different satellite sources. We observed that the amount of bare sediments progressively diminished and the biomass became more dense compared to the existence of sparse biomass in the past. We argue that this is due to the new river hydrology and sediment load imposed by the dam, which increased sediment erosion by deepening the channel. The dam also increased the low flow and reduced peak during flood season reducing the natural oscillations of the water table and the possibility to plant was removed during floods. We also indicate that the new hydrology and reduced sediments have changed, respectively, the downstream (e.g. lake level), and upstream (e.g. mouth bar deposition) boundary conditions controlling the evolution of the delta structure. As a result, the delta morphology became less dynamic and less complex.

Plain Language Summary

This paper studies the river Omo in Ethiopia and lake Turkana in Kenya. . The lake is the fourth largest lake and the largest desert lake in the world. We want to understand the impact that the construction of several dams on river Omo have had on the natural behaviour of lake Turkana. We used satellite imagery to study the area of interest over the past decades. The amount of sediment in the river delta reduced with the presence of dams. These also limited the natural oscillations in the water level of the lake. This meant that local farmers could not plant during flood season, as they used to, after the dams were built. The dams also changed the shape of the river mouth from its natural conditions.

1 Introduction

Fluctuations in lake levels and sediment load carried by the river that flows into the lake are the two main factors controlling lake delta dynamics (Haack, 1996). When a river reaches a basin, the backwater effect modifies the water flow from uniform to nonuniform inducing changes in the flux of channel bed material according to river flow conditions. During low–medium flows, the velocity decreases, suspended sediment is deposited, and the river channel tends to aggrade forming wider cross sections. On the other hand, when the river flow is high, the high velocity promotes channel bed erosion and channel avulsion, generating new fluvial distributary channels (Nittrouer et al., 2012). With time, sediment deposits forming mouth bars can be remobilized during subsequent high flow event thus promoting channel bifurcations (Edmonds & Slingerland, 2007). If the system is not disturbed by external forcing such as waves or tides, the channels of the bifurcation will experience avulsion and form new distributary channels, where a new mouth bar will be deposited originating a new bifurcation. Subsequently, the sediment deposited upstream of the mouth bar will reduce the local slope and increase friction leading to new deposits, and new avulsion. In non–cohesive channels, this cyclic morphological process will result into the autogenic fractal structure that characterizes river delta formations (Kim & Jerolmack, 2008). Therefore, the avulsion time scale exerts fundamental control on the development of a delta network and its length depends on the sediment flux and the length of the channels. The spatial and temporal scales of this cyclic formative process in river deltas have a deterministic behaviour and can be determined as function of the boundary conditions, e.g. lake level (Reitz et al.,

2010; M. Van Dijk et al., 2012). Laboratory observations have shown that when the basin presents high water level, aggradation and in–channel deposition from the mouth bar stop and channel avulsion is inhibited, leading to static distributary channels (Wang et al., 2019).

The presence of vegetation modifies the mechanism presented above for the case of non–cohesive channels by changing the time scales in which bifurcations occur and the overall delta network evolution (Piliouras & Kim, 2019). Plant roots increase sediment resistance to erosion by stabilizing alluvial bars, e.g. channel bifurcations, and reducing bank erosion, while the biomass modifies the local flow inducing sediment deposition (Nepf, 2012). For a quantitative review of this processes see Politti et al. (2018). In turn, plant dynamics are influenced by river processes that select the type and spatial distribution of riparian vegetation (Camporeale et al., 2013; Gurnell, 2014), as well as the development of the root structure (Tron et al., 2015). As a consequence, this affects the resistance offered to sediment erosion (Caponi & Siviglia, 2018) and plant uprooting by flood (Bau' et al., 2019). In addition, the interplay between vegetation growth time scales and flood occurrence control the probability of plant survival and growth (Calvani et al., 2019). In turn, this affects the collapse of vegetated banks (Corenblit et al., 2007), and so the timescale with which channels narrow or widen (Zen et al., 2016; Zen & Perona, 2020). Eventually, the interplay between plant growth and river processes determine biomass spatial distribution within the floodplain and resulting river morphological patterns (W. Van Dijk et al., 2013).

Such mutual feedback between river processes, vegetation, and basin level is ultimately controlled by changes in the climate, particularly temperature and precipitation. Moreover, the effects that changes may have on bio–morphodynamics are further enhanced in arid and semi–arid regions. The challenging environmental conditions for plant development will increase the impact that even small changes in atmospheric conditions, river flow and sediment discharge, could have on the channel morphodynamics, the type of vegetation populating the floodplain and its spatial distribution. Furthermore, high temperature could increase the evaporation rate reducing the water level within the basin receiving the river flow and sediments. Lake Turkana and the lower Omo River constitute an example of such environment, where in addition to precipitation and river flow, the lake level plays a crucial role on the control of the eco–morphodynamics of the floodplain. In a study conducted by combining early Landsat imagery and local field observations, Haack (1996) showed that the lake level had dropped around 10 m from 1973 to 1989 allowing the formation of a large wetland and an estuary at the lake inlet. An aerial survey revealed that the delta was covered predominantly by grasses on the order of 1–2 m in height, and trees and shrubs on river levees, as well as a high sediment load within the Omo River. According to the author, such high presence of sediments was generated by an increased sediment erosion in the upper part of the Omo basin due to deforestation.

Few years later, Carr (1998) described the delta area as characterized by seasonally inundated mudflats, and swamp grasslands of mixed aquatic and semiaquatic species (e.g. microphytes), with overflow from the bank typically occurring during flood season between August and September. A typical river bank within the lower Omo and the channels forming the delta presented aquatic and semiaquatic vegetation close to the water, and mesophytic grasses in the middle of the bank, while the bank crest and its downslope were covered by grassland and sparse shrubs and trees. Among the woody vegetation, the most common was, *Ficus sycomorus*, which could reach up to 15 m, but their development was prone to river overflow able to cover half of their trunk generating anoxic conditions. Because of this, the presence of woody species, as well as forest density, increased while moving upstream from the lake. For more details in the type of vegetation colonizing floodplain and channel banks of the lower Omo River, see Carr (1998).

A study conducted on a flood in 2006 showed that due to the increased intensity of local rain events associated to higher temperatures, and the augmented sediment erosion due to deforestation, floods have increased their capability to modify the floodplain by eroding banks, removing vegetation and depositing sediments. This resulted in changes of

the morphology of the sinuous–meandering lower reach of the Omo River, as well as the channels forming its delta (Ayalew, 2009). In addition to the changes in the local climate, the river and lake dynamics have been modified in the last decades by the construction of three dams within the Omo basin: the Gibe I, Gibe II, and Gibe III dams. Particularly, the Gibe III dam is the latest dam of the energy plan, it is 243 metres high and presents an installed power of 1,870 MW. The dam work started during 2006 and became operational in December 2016 (Avery, 2012). The effect of these dams in the surrounding environment has been source of public debate. A recently published paper analysed the filling process of the Gibe III dam, which caused a drop in the water level in Lake Turkana of 1.7 m, (Zaniolo et al., 2021). The paper provides quantitative evidence of the benefits generated by adaptive filling strategies, attaining levels of hydropower production comparable with the historical ones while curtailing the negative impacts to downstream users.

In this work we aim to quantify the impact of lake level changes on the eco–morphodynamics of the Omo River delta, and to seek for possible correlations to to either or both climate variations and dam works. First, we aim to quantify the temporal changes in land use and atmospheric forcing occurred within the study area. Second, we analyse the historical series to assess what has induced such changes, namely: a new river hydrology imposed by the dam, or changes in the climate of the area. Third, we observe the river morphological structure throughout the time frame investigated to quantify river morphodynamics and relate this to the changes mentioned above.

2 The study area

The Turkana Lake is located in the Northern–Western Kenya, at the border with Ethiopia, Africa. The lake is characterized by a long shape oriented north–south, the distance between the north shore and the south shore is around 200 km and the maximum width is around 40 km. With a surface of almost 7,000 km^2 the Lake is the fourth largest lake in Africa and the world largest desert lake. It has a mean depth of 31 m, and a maximum depth of 114 m. The lake is fed by three rivers, the Turkwel and Kerio Rivers from the South–West, and the Omo River from the North. The latter provides almost the totality of the lake inflow (90%) and flows through Ethiopia. When reaching the lake, the Omo River deposits sediments originating a branching structure (see Figure 1). The Omo River shows a humid hydrological regime with an average annual rainfall estimated around 310 mm while the desert area of the Lake shows a much lower annual rate around 200 mm, which results in an average precipitation of 0.5 mm/day. Conversely, the Lake is characterized by a strong evaporation rate, which has been estimated to be around 7 mm/day (Avery, 2012). The evaporation process is enahnced by a strong South–Eastern wind, which also generates strong secondary currents that contribute to diffuse the sediments carried by the Omo River deeper into the lake and along the North–East shore.

The natural inflow of the Omo River is characterized by a flooding season between August and October with a maximum flow discharge of about 1,650 $m^3 s^{-1}$. Following dam operations the new river regime is characterized by two peaks occurring in May and October, which have been estimated to be around 680 $m^3 s^{-1}$ and 1,200 $m^3 s^{-1}$, respectively (see Figure 2). In addition, the modified flow presents a low flow regime, occurring during winter time and in July more than twice that of the natural flow of 200 $m^3 s^{-1}$ (Avery, 2012).

Downstream the large bifurcation of the Omo River, the vegetation is less impacted by human activities compared to the area upstream and more regulated by the river hydrology Carr (1998). Therefore, in this work we focus on the changes associated to the delta area and surrounding shores corresponding to the upper portion of the lake as showed in Figure 1, panel c). The area does not extend further upstream to avoid the inclusion in the analysis areas of the Omo floodplain characterized by cotton crop fields. Indeed, the presence of crops

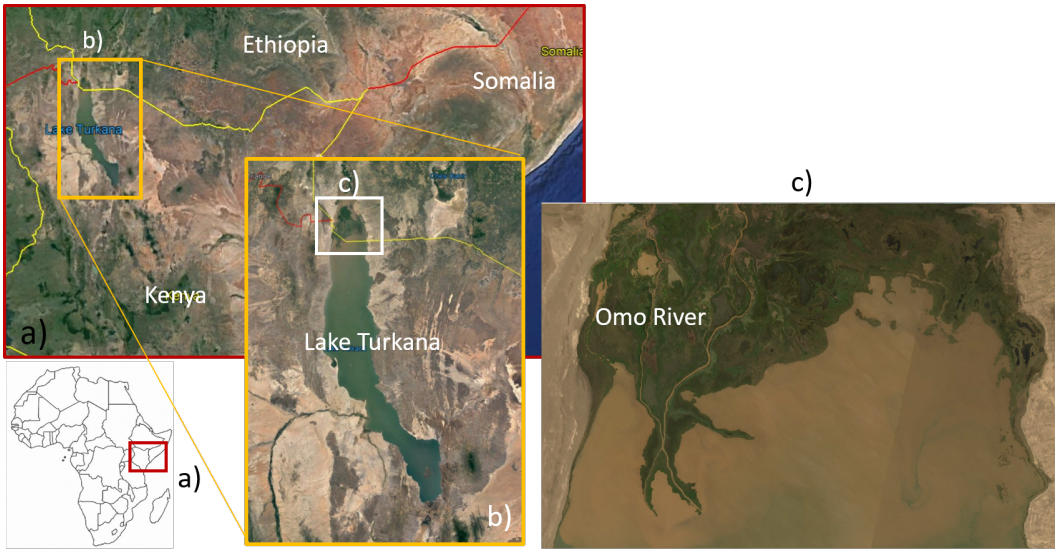

Figure 1. The study area at different zoom levels, a-c. In c), the Omo river delta clearly appears with its characteristic branching structure.

Table 1. Historical dataset used for the analysis.

Source	Type	Resolution	Interval
Landsat 5	Multispectral	30 m	1986 – 2002
Landsat 7	Multispectral	30 m	2003 – 2012
Landsat 8	Multispectral	30 m	2013 – 2019
ERA5	Reanalysis	0.1^o *	1979 - present

* Spatial resolution of 9 km at the latitude of the case study.

will prevent a correct estimate of the spatial structure of the natural vegetation covering the river floodplain and delta.

3 Materials and Methods

3.1 Historical dataset

A historical dataset was collected by combining data extracted from satellite imagery with historical data on atmospheric variables. In particular, satellite data was used to quantify spatial and temporal changes in land coverage and river/delta morphology. While the historical evolution of atmospheric variables was used to assess the impact of external forcing on the observed changes within the studied area. To extend the length of the time frame covered, we combined different Landsat missions. Information on external forcing of the ecosystem, namely, precipitation, temperature, evapotranspiration from water bodies, land, and vegetation, were collected from the ERA5 dataset provided by the European Centre for Medium-Range Weather Forecasts (*ECMWF*, 2021). A summary of the sources used for the analysis is reported in Table 1.

Since the launch of the first Landsat mission in 1972 the joint program of the USGS and NASA has imagined the Earth's surface twice a month, by collecting different spectral bands of surface reflectance. The first four missions recorded 4 spectral bands: two bands in the visible spectra, red and green, and 2 bands in the short infrared range. The more recent 5, 7 and 8 missions increased the bands recorded from the satellite sensor by including the blue and near infrared bands, and mission 8 also added a ultra blue band, as well as

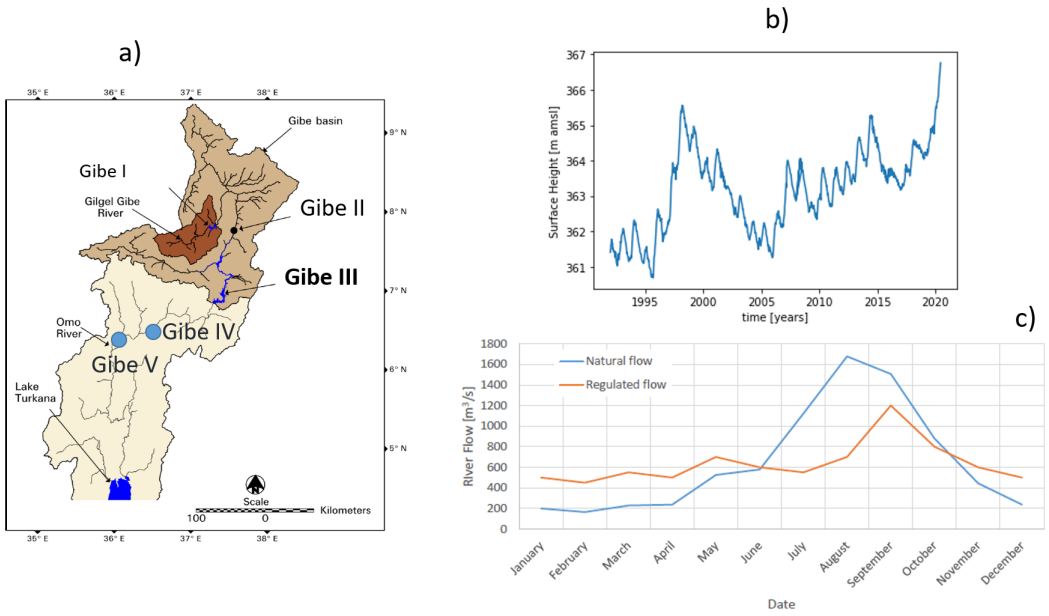

Figure 2. Frame a) shows the Omo River catchment and the location of the Gibe I, Gibe II, and Gibe III dams. The picture shows also the location of the future dams Gibe IV and Gibe V that will complete the hydroelectric development of the catchment (adapted from Avery (2012)). Frame b) depicts the water level measured from satellite altimetry. Frame c) shows the natural flow in the Omo River and flow after the Gibe III dam was built.

two bands associated to temperature. For the presence of the infrared band, the Landsat 5 mission was the first one to allow multispectral images of the study area to be collected since 1986. Since Landsat 7 and 8 provide higher resolution both in space and time, and even more bands, we progressively collected images from more recent missions as soon as the data was available. For each image collected we used the surface reflectance atmospherically corrected product. A total of 200 images were collected covering the time interval 1986 – 2019.

In contrast to direct satellite observations, the ERA5 (ECMWF Atmospheric Reanalysis 5) dataset contains data from the reanalysis of the global climate for the European Centre for Medium-Range Weather Forecasts (ECMWF). The project combines physical–based models with observations across the world to provide high–resolved historical data available from 1979 to three months from real–time. Particularly, we used the monthly–mean values provided by the ERA5-Land dataset which focuses on land variables, including temperature, rain, snow, heat flux, evaporation, and ice (Muñoz Sabater, 2019). For this analysis, we investigated the following parameters: 2 m air temperature, precipitation, evaporation from water, bare soil, and canopy.

3.2 Image analysis

For the geo–spatial study, we analysed data available on the Google Earth Engine platform (Gorelick et al., 2017) using different Python libraries. Landsat imagery provides surface reflectance information corrected from the distorsion induced by the atmosphere that generates a difference between the reflectance value measured at the top of the atmosphere and that measured at the Earth's surface. Therefore, reflectance values can be directly used to quantify the temporal evolution of the study area for each date observed.

Land Coverage

The study area was classified into four classes of land coverage, namely: water, bare ground or sediments, shrubs or young vegetation, and mature vegetation. It should be noted that the water class is then further divided into lake and river or water flooding the floodplain. This difference allowed the lake to be masked from the analysed image. In order to separate water from dry land and then quantify the portion of dry land covered by sediments or vegetation, we computed vegetation and water indices. For the first index, we used the Normalized-Difference Vegetation Index (NDVI) (Rouse et al., 1974), while for the second we adopted the Automated Water Extraction Index with No Shadow (AWEInsh) (Feyisa et al., 2014). Both indices are a linear combination of different reflectance bands and are computed as follows:

$$NDVI = \frac{\rho_4 - \rho_1}{\rho_4 + \rho_1} \quad (1)$$

$$AWWEInsh = 4(\rho_2 - \rho_5) - (0.25\rho_4 + 2.75\rho_7) \quad (2)$$

where ρ_1 is the red band, ρ_2 is the green band, ρ_4 is the near infrared band, ρ_5 is the shortwave infrared band 1, and ρ_7 is the shortwave infrared band 2. Positive values of AWEINsh and NDVI are associated, respectively, to wet and dry pixels.

Among the various water indices that have been proposed in the literature, the AWEInsh index shows high efficiency in identifying mixed pixels in absence of signification elevation changes and when in the scene there are no shadows provided by mountains or buildings, nor snow (Acharya et al., 2018). Mixed pixels are typical of rivers and lake shores, where in shallow waters the presence of suspended sediments, chlorophyll or shore vegetation could lead to pixel misclassification. Once the wet land was separated from the dry land, the distribution of the positive NDVI values extracted from each pixel was obtained for each available date. This allowed us to compute the principal moments of the distributions, obtaining a value of mean, variance, and skewness for each collected images of the dataset.

The typical distribution of NDVI values, for the study area, is a multimodal distribution with three peaks. Therefore, we classified the dry land portion into bare ground, shrubs or young vegetation and mature vegetation, considering that mature canopy presents more foliage and thus higher NDVI values. In a study conducted on a riparian environment in the temperate zone, Henshaw et al. (2013) identified NDVI values lower than 0.2 with bare ground and greater with vegetation. Another study conducted over a period of 13 years on different types of vegetation for a north-Africa semi-arid region Amri et al. (2011) observed that, on average, NDVI values were comprises between 0.2 and 0.4 for shrubs, pastures and sparse small trees, with extreme seasonal values ranging between 0.2 and 0.5. An analysis on the efficacy of vegetation optical depth to estimate vegetation green biomass in African drylands presented an NDVI in the range 0.2-0.5 for low values of biomass that progressively increased when biomass increases. Particularly, when woody canopy occupied more than 10% of the study area the NDVI values where higher than 0.4 (Tian et al., 2016). By considering these values, a pixel was classified as bare ground when $0 \leq NDVI < 0.2$, shrubs if $0.2 \leq NDVI < 0.4$, and mature vegetation when $NDVI \geq 0.4$.

Because wet sediments can be detected as water when analysing multispectral imagery, water and bare ground classes were joined together in order to compare different land coverage in the signal analysis. Few preliminary operations were required before analysing the satellite imagery. Due to a failure of Landsat 7's Scan Line Corrector, since 2003 Landsat 7 images were not collected following a straight path but a zigzag path, which resulted in the black stripes of missing data characterizing images from Landsat 7 (*USGS-Landsat7*, 2021). Therefore, a 5-pixel square window was moved around the whole image and the median of the neighbours was assigned to the central pixel. The original image was then superimposed on top of the filtered one to keep the resolution of the original image where possible. Finally,

images presenting a cloud coverage value greater than 5% were rejected at the beginning of the analysis.

River morphology

Changes in river and lake delta morphology throughout the time frame considered in the analysis were analyzed. First, the lake was masked from the image on the base of the AWEInsh value, leaving the shore and the river because of their shallow water (which generated lower values of AWEInsh). Second, a combination of the AWEInsh and NDVI were applied to the new masked image to extract a binary image of the river, i.e. pixel values 0 and 1 were associated to land and water, respectively. Third, the binary image obtained was analysed by using morphological operations (e.g. erosion, dilation) to get rid of wet portion of land and further isolate the river structure. Once the river structure was available, the number of bifurcations from the main channels were computed as proxy of morphological activity. In this count, we included any bifurcation within the main channels as well as river branches associated to an anastomized pattern and those characterizing the fractal structure of the river delta. However, due to difficulties in completely removing wet areas close to branches of the Omo River, the counting operation was made manually, once the river structure was clearly outlined.

3.3 Time series analysis

The historical time series of land coverage and climate variables were analysed to explore relationships between changes in land coverage, amount of precipitations, air temperature, and evaporation rate. Before doing this, a preliminary operation was required to re-sample all the signals to the same one-month time interval. Because data extracted from Landsat missions did not allow a constant sampling frequency, the signal extracted from the analysis of the multi spectral imagery was interpolated using splines interpolation and data was re-sampled using a monthly time interval, in order to match the same time resolution of the ERA5 dataset. Such newly generated signals were then used to explore changes in the period before and after the construction of the dam began. Since the works to built the dam started during 2006, we chose the 1st January 2007 as a date from which dam building operations could have impacted the water and sediment dynamics in the downstream river reach and its floodplain. A further comment is however in order here. Following the start of the construction works in 2007, the dam became operational only many years later. As a consequence, the results of our analyses for the "postdam" period will actually be damped by the inclusion of the time series recorded during the construction time.

A Fourier analysis was conducted on the one-month resolution signals and the first five frequencies characterized by higher power spectrum were used to low-pass filter the series. The filtered signal, almost deseasonalized, was assumed to be representative of the trend. In order to perform this analysis each signal was repeated 20 times to introduce periodicity and obtain a long time series more suitable for the Fourier analysis. The auto-correlation function was computed for all the land coverage signals, before and after the Gibe III dam, to quantify temporal changes associated to the presence of the dam. Since low frequencies, i.e. seasonality, temporary induced correlation within the signal, the original signal was filtered by keeping only the higher frequencies. This was achieved by subtracting the long term trend obtained through the Fourier analysis to the original signal.

Because changes in land coverage may be associated also to changes in weather conditions, we compared the time evolution of land cover with that of the atmospheric variables. First, we computed the annual minimum, mean, and maximum of air temperature, evaporation from sediments and evaporation from vegetation. Second, the cross-correlation function was computed for the following couple of detrended signals: shrubs and water, mature vegetation and water, shrubs and temperature, and mature vegetation and temperature. By considering that sediment and water coverage are mutually dependent, i.e. if water increases

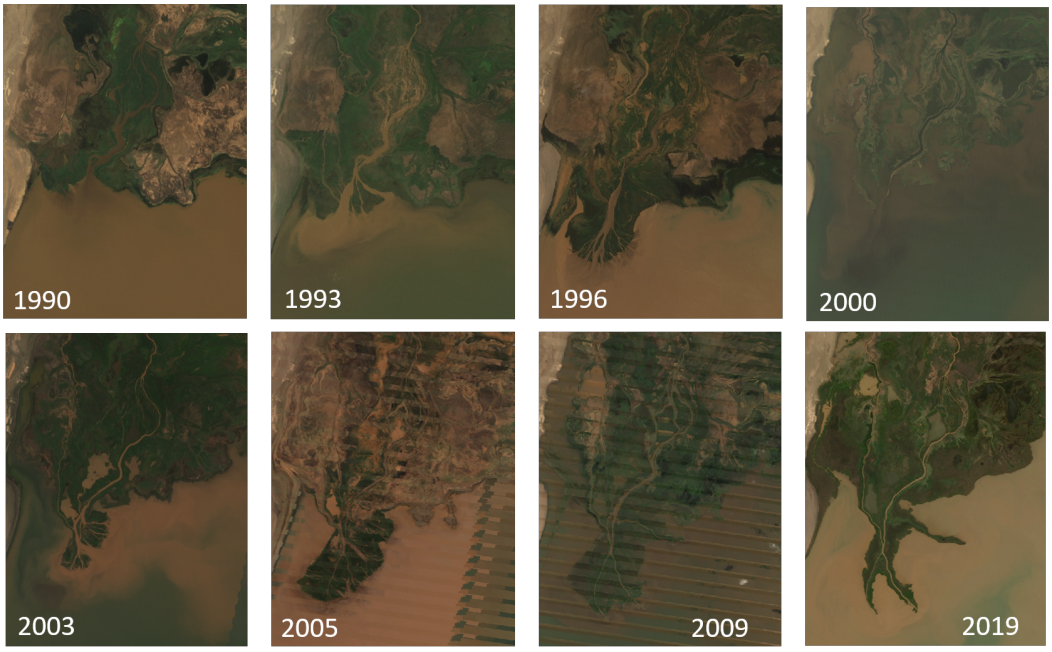

Figure 3. Historical sequence showing the evolution of the study area as observed from satellite imagery.

dry sediment portion decreases and vice versa, in computing the cross-correlation function, water and bare ground time signals were combined together. Henceforth, we will refer to this combined signal as to the non-vegetated signal.

A linear correlation analysis was conducted on the detrended signal. This would allow to assess the level of noise affecting the series and then upon occurrence to remove it by using, for example, autoregressive models (Głogowski et al., 2021). However, this operation was done only for those variables sampled with sufficient high resolution, e.g. like the environmental ones. Finally, in order to compare different variables, all the detrended signals were preliminary standardised, by subtracting their mean and dividing the result for their standard deviation.

4 Results

Figure 3 shows a discrete temporal sequence of satellite images of the domain being studied. To notice, are the early formation of the delta in 1993, and its subsequent development until the period of high water level (panel related to year 2000 in Figure 3) as seen in Figure 2b. After shore and floodplain were flooded, the river modified its course and delta structure (years 2003, 2005 in Figure 3). Later, a less complex delta structure appeared, and the river presented an almost single thread channel upstream, with an anastomosing section and a bifurcation before reaching its delta, which at this stage was reduced to two main channels (year 2009 in Figure 3). The latter channel morphology is kept unchanged in the following years, while a substantial erosion of the sediments forming the delta occurred (year 2018). The diagonal lines in the panels associated to year 2005 and 2009 are the result of the interpolation conducted to fill the stripes with no data due to a malfunctioning of the sensor on board of the Landsat 7 mission.

The multispectral imagery, of which their RGB (Red-Green-Blue, or visible) bands combination is presented in Figure 3, were used to estimate the water and vegetation index,

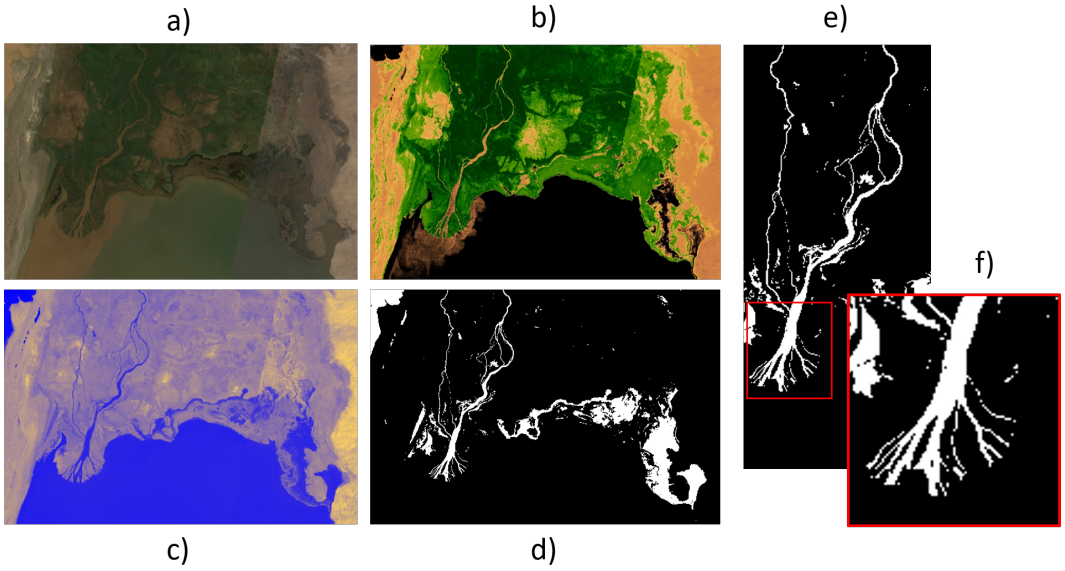

Figure 4. Example of the image analysis conducted for the study area. a) RGB image, b) NDVI, c) AWEInsh, d) lake waters masked from the wet portion, e) river structure, and f) close up showing the details of the delta morphology.

AWEInsh and NDVI, respectively. These two indexes were used to asses the land cover type for the different dates available, and to separate the Omo river from the Turkana Lake. An example of the image analysis conducted is reported in Figure 4. Figure 4a shows the RGB image. Figure 4b and c show the distribution of the NDVI and AWEInsh values, respectively. Colours in Figure 4b go from 0 to 1, such that pixels below or equal to 0 appear black. Although these values are usually associated to water, it can be noticed that in Figure 4b the Omo river and the delta area do not appear black. This is essentially due to the presence of suspended sediments and macrophytes within the Omo River that induce higher reflectance of the NIR (Near-Infra-Red) spectrum compared to that observed for clear water. This is also supported by the diffusion observed around the delta, indicating the release of solid transport from the river to the lake, compared to the sharp border identified in the AWEInsh image (Figure 4c). This latter index allows to clearly identify the lake border and the main channel of the Omo River, but barely detect the presence of secondary channels in the anastomosed section. Therefore, AWEInsh was used to mask the portion of the study area covered by the lake, and a combination of the NDVI values with AWEInsh values was used to extract the morphology of the channel as reported in Figures 4d, e, and f.

The analysis of satellite imagery allows to quantify spatial and temporal changes in land coverage and the results were presented as percentage of the study area. Such results are reported in Figure 5a-d along with the other historical series for precipitation (Figure 5e), temperature (Figure 5f), evaporation from water (Figure 5g), evaporation from bare soil (Figure 5h), and evaporation from vegetation (Figure 5i), that were collected from ERA5 dataset. Each panel presents in blue the original signal and in orange the long term signal filtered from the higher frequencies. Time signals that describe the evolution of system variable in natural systems are characterized by a medium-long term trend and short-term events. Therefore, each signal can be decomposed into a deterministic and a stochastic component. The long-term component of each analyzed signal is reported in orange in Figure 5. The filtered signal shows the Fourier series of the first five modes characterized by

highest power spectrum. Such signal represent the seasonality of the variable. The analysis highlights a progressive rise in air temperature since the year 2000 and an increase in the evaporation from the vegetative compartment since the yer 2008. After 2006, water coverage shows an increasing trend, opposite to sediment and young vegetation that progressively decrease, with the study area showing almost no bare ground spots by the end of the time period analysed. Conversely, mature vegetation shows an almost constant trend after 2008.

Around 1997 an increase in the annual rainfall of about 380mm/yr (Avery, 2011) determined a high water level in the lake and the Omo River, with consequent overflow and inundation of a great portion of the study area (see Figure 5d). After this event the rain events showed an increasing trend, which possibly kept a high level within the river and lake (Avery, 2011). This induced an abrupt diminishing in vegetation, for both classes, as well as for the dry bare ground area (see Figure 5 b,c,d). However, while the amount of exposed sediments recovered fairly immediately to its original value, both shrubs and mature vegetation required a long time to recover to their previous condition. It should be noted that such recovery trend is inverted for shrubs around 2007 without allowing this vegetation type to recover to the same area occupied in the early 1990s before the inundation period took place. On the other hand, mature canopy recovered to its previous status, which it kept almost constant after 2007. The amount of exposed sediments keep oscillating until around 2008 when the portion of dry bare ground start to decrease until almost completely disappearing. The portion of land lost by shrubs and dry sediments seems to be substituted by water and mature vegetation.

The analysis of the historical trend for the environmental variables extracted from the ERA5 dataset, namely air temperature, and evaporation from soil and vegetation, are reported in panels e), f), g), h), i) of Figure 5. These data show an increase in air temperature after 2003, while the evaporation from wet surface remain unchanged over time. The amount of water evaporating from the soil surface shows a medium-long term signal with a regular pattern and a frequency of about 5 years, as well as high frequencies with values progressively decreasing after 2006. On the other hand, the medium-long term signal of the evaporation from vegetation shows a frequency of about 3 years, while the high frequencies present values that slightly increase after 2006.

This behaviour is better shown in Figure 6, where the yearly minimum, maximum, and average values are presented for air temperature, evaporation from soil, and evaporation from vegetation in Figures 6a, b, and c, respectively. The average annual temperature presented an oscillatory pattern with a frequency of 10 years until 2003, and an almost constant value around 29^oC after. This is possibly due to a combination of the high maximum temperatures recorded between 2007 and 2009, and the high minimum temperatures observed between 2009 and 2015, of about 29^oC. The average annual value of the water evaporated from the canopy followed the temperature pattern, with the same 10-year oscillations: maximum and minimum values around 1986 and 1996, and 1991 and 2001, respectively (see Figure 6c). After 2003, the oscillations are minimal and the average evaporation from trees was around $3.5\ 10^{-3}$ m. Also in this case, there was a consistent increase in the minimum annual evaporation after 2003. Conversely, the annual average of water evaporated from the bare soil was not aligned with the air temperature trend (Figure 6b). First, the values before 2003 are anti correlated with those of temperature. Second, the average values decreased between 2006 and 2011 to a value of $0.5\ 10^{-4}$ m, and started to oscillate around an evaporation of $0.6\ 10^{-4}$ m with a frequency of 5 years. This decreasing trend is also evident in the maximum annual values, while the minimum values of evaporation remained almost constant trough the time frame explored.

All time series were split into two signals before and after the start of the construction works of the dam, whose reference date was chosen to be 1st January 2007. The autocorrelation function was performed on the detrended signals. Results are reported in Figure 7 for the land coverage signals before (blue line) and after (red line) the start of the works. All

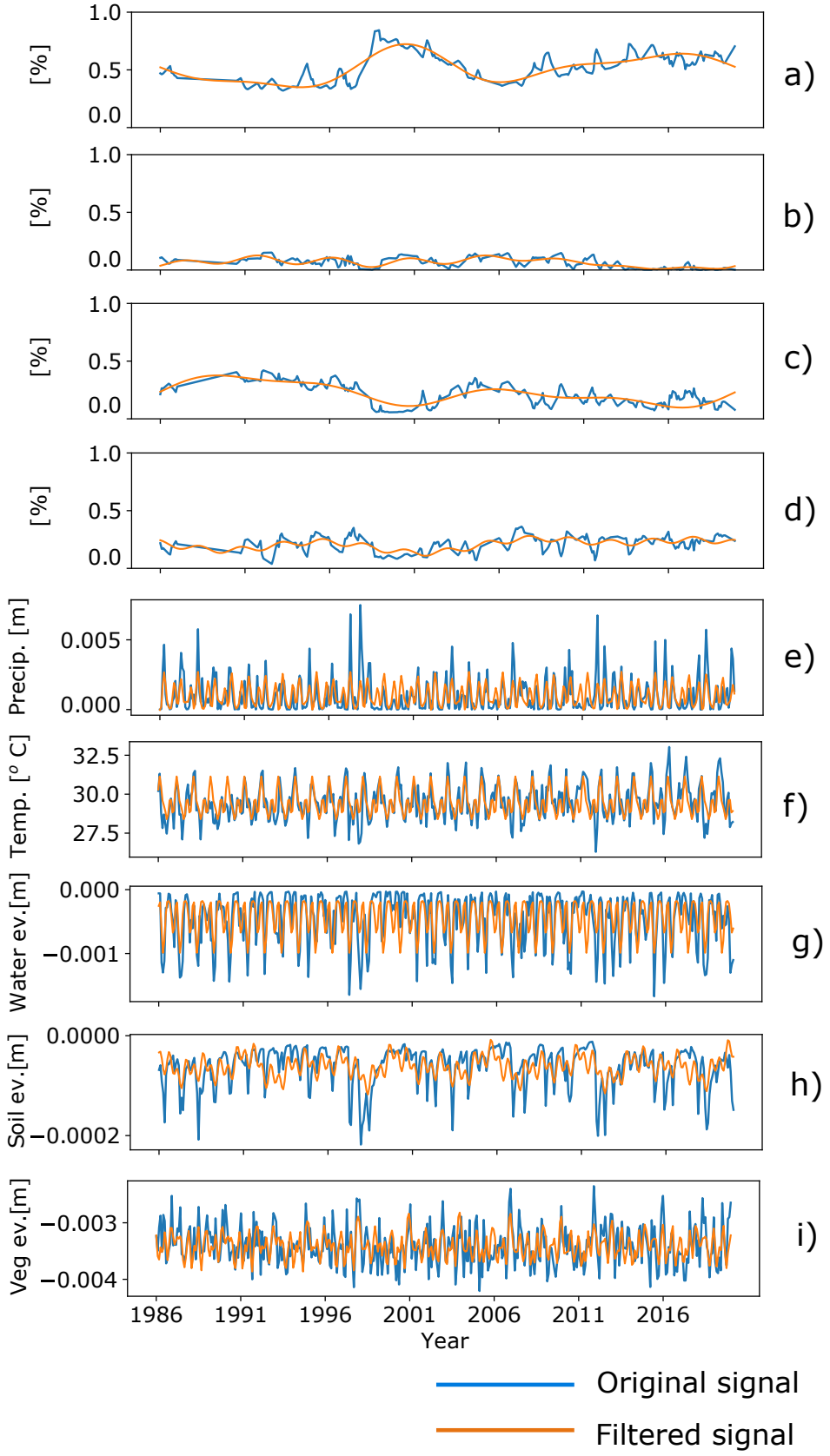

Figure 5. Historical series of land coverage and atmospheric variables extracted from satellite data for the time period 1984-2019. Blue and orange line indicate original and filtered signal, respectively. Panels a-d present changes in land coverage within the study area observed by combining images of Landsat 5,7 and 8, with a) showing the wet land, and the dried land divided into b) bare ground, c) shrubs or juvenile vegetation, and d) mature vegetation. Panels e-i show the time series extracted from ERA5 data for the study area: e) precipitation (m), f) temperature (°C), and g), h) and i) the cumulative amount of water evaporated in one month from water, bare ground, and vegetation.

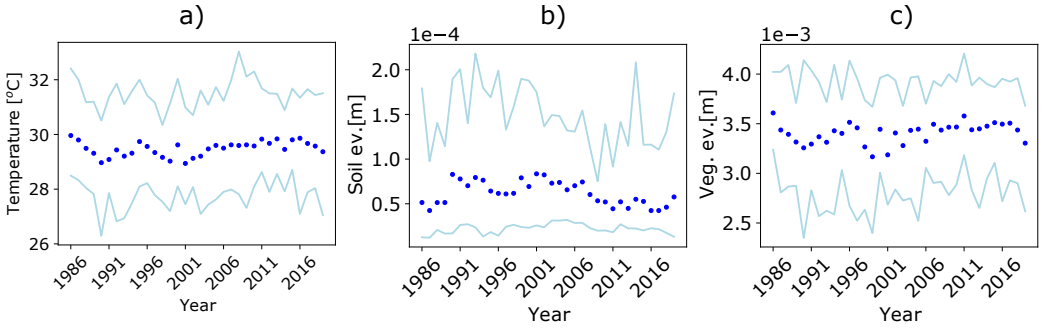

Figure 6. Annual average (dotted line), minimum and maximum (solid lines) for a) air temperature, b) evaporation from bare soil, and c) evaporation from canopy.

the autocorrelation functions reported in Figure 7 show a structure representing a temporal correlation that operates at annual and seasonal time scales.

Panel a) of Figure 7 shows no changes between the two periods, while b) and d) show that, respectively, the signals for sediments and mature vegetation lost correlation after the starting of the construction works, with the dynamics of the bar ground surface presenting a lag shift of almost 5 months between the pre- and post-dam scenarios. Likely, this earlier decorrelation of the bare ground surface explains the appearence of a peak of annual correlation in young vegetation in the post-dam period (Figure 7 c). Accordingly, shrubs and mature vegetation showed changes in their autocorrelation structure before and after the construction of the dam (Figure 7c and d), but the average temperature of the area also increased during a very similar period (see Figure 6a) and may have influenced these two dynamics as well.

Vegetation dynamics could have been impacted by changes in fluvial processes, i.e. river flow and sediment load, due to the construction and operation of the dam, but also by variations in temperature (Figure 6a). For this reasons, time series associated to vegetation type were compared with the non-vegetated signal (sediment and water) and temperature time series. Figure 8 shows the cross-correlation function for the following couple of variables: non-vegetated and young vegetation (Figure 8), non-vegetated and mature vegetation (Figure 8b), temperature and young vegetation (Figure 8c), and temperature and mature vegetation (Figure 8d). As for the autocorrelation function above, also the cross-correlation function was computed for the period before and after the dam construction.

Panels a and b of Figure 8 show that vegetation is inversely related to changes in water and sediment. Although water and sediment signals are combined, the changes in water coverage have a dominant effect in controlling the overall trend of the combined signal. This means that when water level increases vegetation decreases. However, this behaviour is modified after the dam was built, with the two signals being correlated for half of the time they were previously correlated. Figure 8 c and d show that the cross-correlation function between vegetation coverage and temperature also presents a structure. This means that the monthly resolution with which data are available introduce a within-signal correlation that operates at the time scale of one year. Although, from 2003 the average temperature has increased (Figure 6a), the cross-correlation functions between vegetation and temperature did not change before and after the dam (2007).

Further investigations on land coverage changes were conducted by analysing the temporal evolution of NDVI values. The analysis of the distribution of NDVI values within the study area per each date observed revealed an increasing average after the dam was built

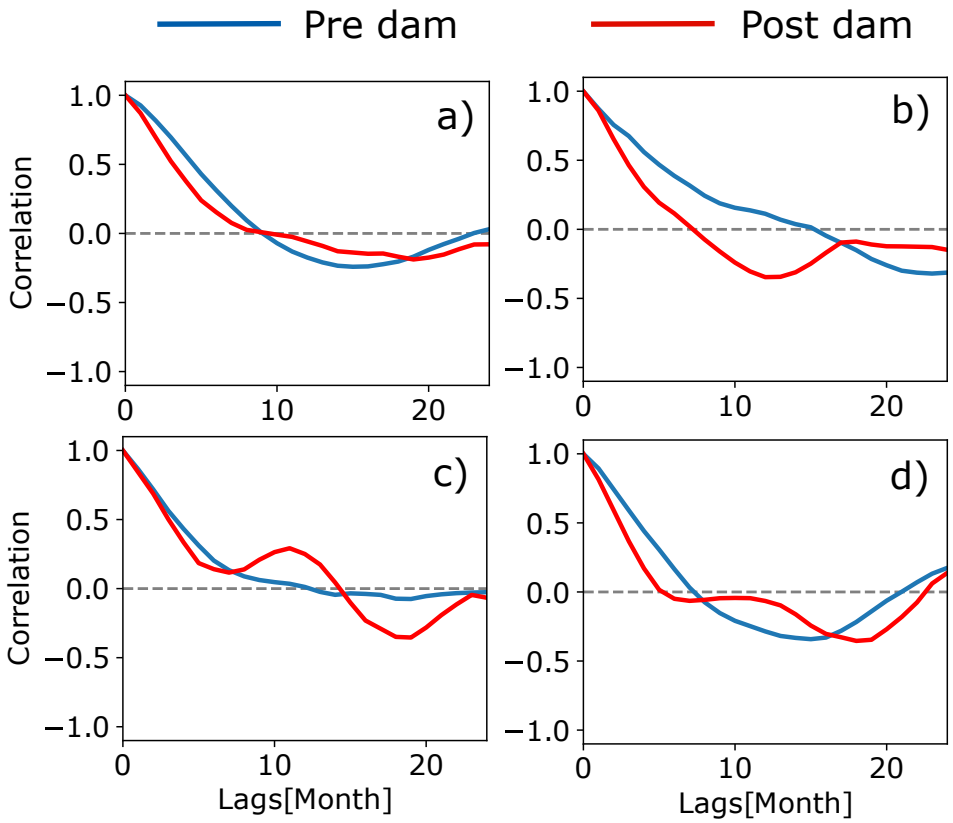

Figure 7. Autocorrelation function for the land coverage signals a) water, b) bare ground, c) shrubs, and d) mature vegetation; for the period before and after the Gibe III dam was initially built reported in blue and red, respectively.

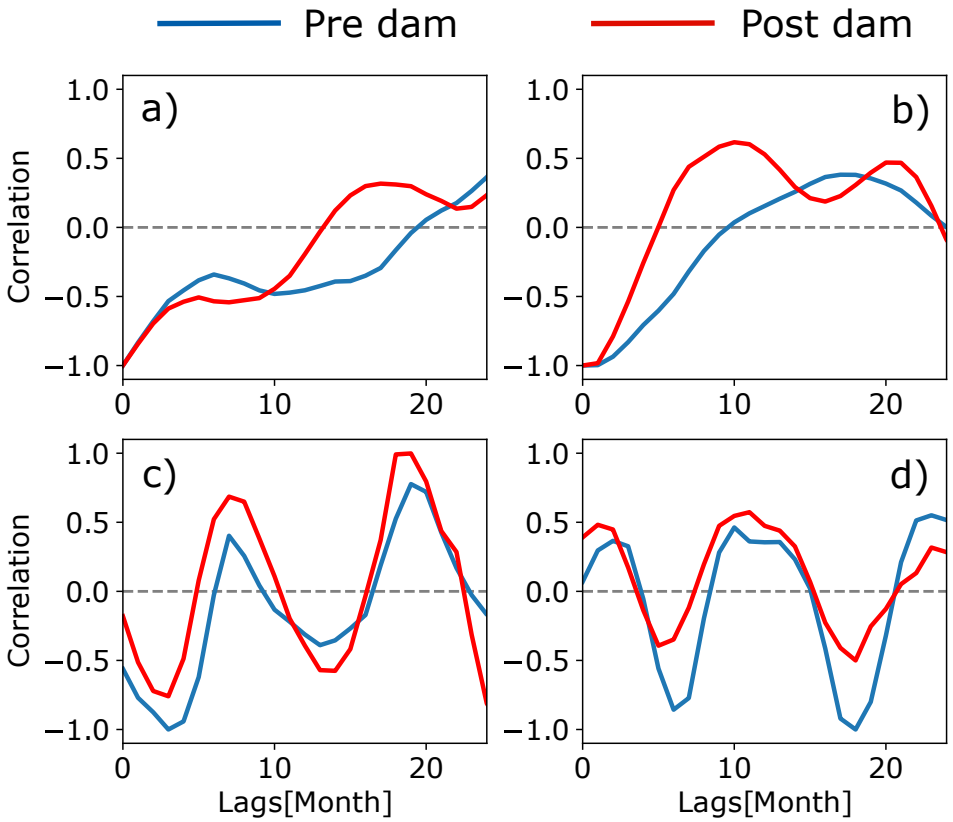

Figure 8. Croos-correlation function for the land coverage signals a) sediment weater and shrubs, b) sediment and water and mature vegetation, c) temperature and shrubs, and d) temperature and mature vegetation; for the period before and after the Gibe III dam was initially built reported in blue and red, respectively.

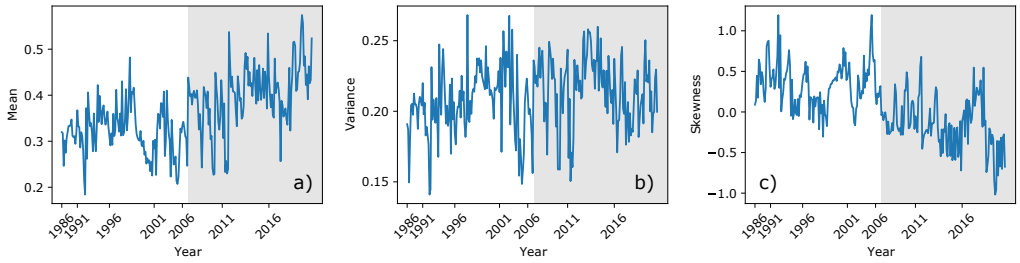

Figure 9. Major statistics of the NDVI values distribution for the dates images were available. Shadow background indicates the presence of the dam (construction started in 2007).

(Figure 9a). More interesting are the results obtained for the third moment of the NDVI distribution, which shows how the vegetation distribution has been progressively skewed toward mature vegetation after the dam was built, i.e. negative skewed. Nevertheless, the variance values for the same distributions have not changed during the time frame considered in the analysis. This means that young vegetation persist in the study area even after the construction of the dam, but it saw the portion of land occupied shrinking after 2007.

Figure 10 presents the morphological evolution of the river and its delta through the time period considered in the analysis (panels of Figure 10a and close ups on Figure 10b). Panel c shows the value of the morphological index, which indicates the number of bifurcations observed for the river segment and delta within the study area. Figure 10 clearly shows how after the construction of the dam in 2007 (gray shade in the plot) the river progressively diminished the complexity of its morphological structures both as number and variability in time. Before the dam was built, the river was highly dynamic with a lot of secondary branches that were destroyed and generated during floods. This is supported by the variations observed in Figure 10c before year 2007. In this pre-dam phase, the abrupt decrease in number of channels is associated to an increase in the lake level that overflow the floodplain for few years as it can be seen in Figure 5a. The post-dam period (grey background in the plot) is characterized by smaller variations in the number of channels with a channel hyper simplified and almost unable to evolve after 2016 (i.e. almost constant 3 bifurcations).

5 Discussion and conclusion

5.1 Changes in climate variables and boundary conditions

Figure 5e shows an increasing frequency in large rain events after 2009. This may have lead to a higher flow in the Omo River and, consequently, to a deeper lake level, as suggested also from the positive trend of the percentage of wet study area (Figure 5a). Measurements of lake level from satellite altimeter (USGS) revealed that the lake level has constantly increased after the dam became operational in 2016. Indeed, the hydrograph in Figure 5e shows how the dam released in the lake a larger discharge compared to the natural one for the majority of the year. However, simulations conducted to explore the impact of the Gibe III dam have revealed that the increase in water level observed within the last decades is less than the rise that the lake would have experienced if fed by a natural inflow. Nevertheless, the level rise may have hampered the deposit and avulsion cycle that guides delta development (Wang et al., 2019), since the delta first originated during a much lower level of the lake in the 1970s (Haack, 1996).

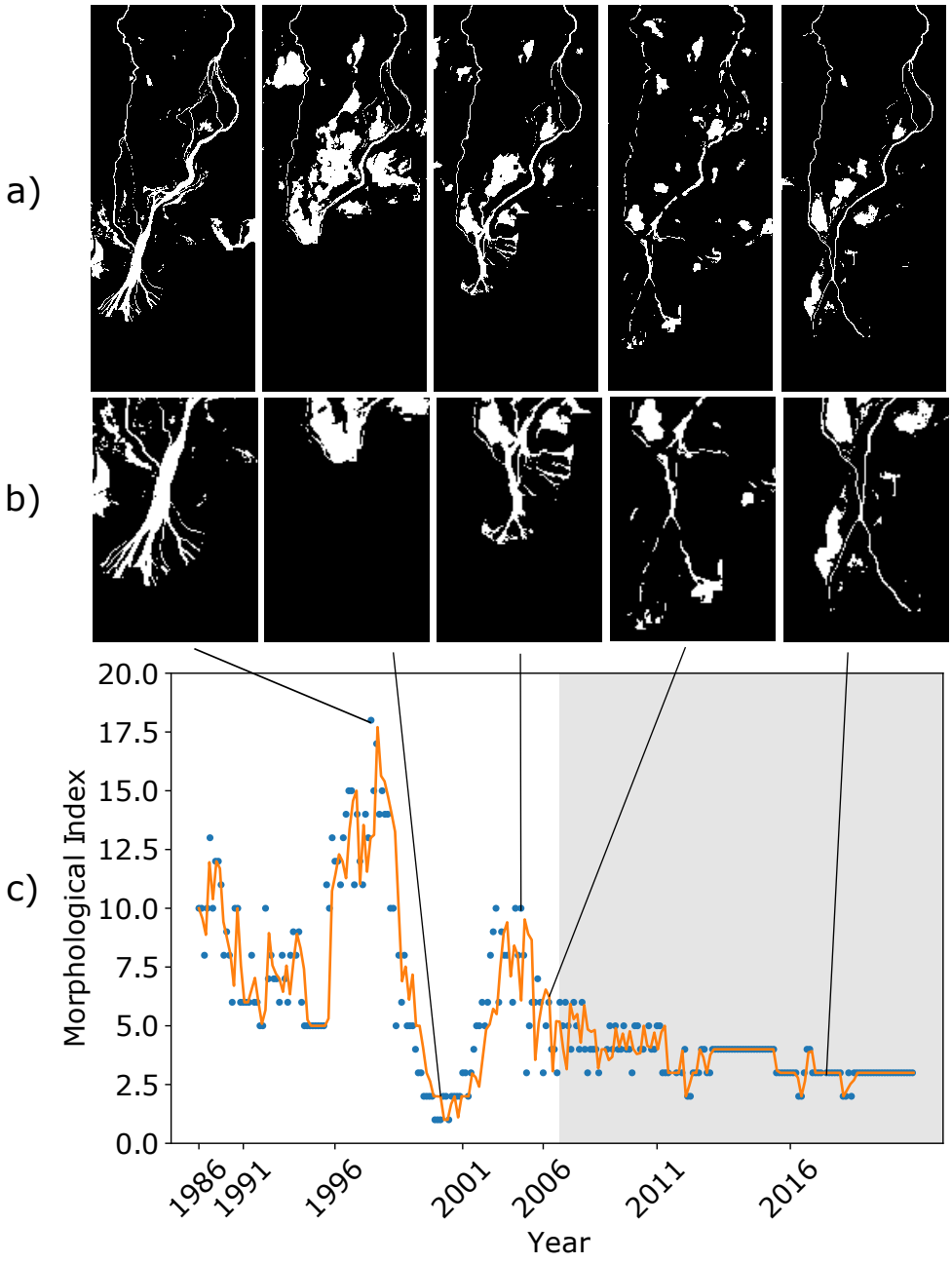

Figure 10. River morphodynamics of the lower reach of the Omo River as observed from the satellite images. Panels show a) the lower reach of the Omo River, b) a close up with the detail of the delta structure, and c) the temporal evolution of the river planform where the number of bifurcations, i.e. morphological index, is used as proxy of morphological processes.

The rise in the annual minimum and average temperature after 2003 (Figure 6a) is associated to a decrease and increase of the evaporation recorded from the bare soil (Figure 6b) and vegetation (Figure 6c), respectively. While the former is due to a reduced amount of dry bare sediments, the increase in evaporation from vegetation could be given by the increase in temperature observed. The cross-correlation function computed for the couple vegetation-temperature for the period before and after the dam revealed no changes in the cross-correlation structure (Figure 8c and d). By considering that changes in air temperature were observed starting from 2003 and the after-dam period started in 2007, we can argue that temperature may have increased the evaporation from vegetation, but it was not responsible for changes in vegetation dynamics.

5.2 River and delta morphodynamics

The morphology of the lower reach of the Omo River has experienced large changes within the past 50 years (Haack, 1996). The historical dataset collected in this analysis showed how the river was morphologically active with an anastomosing pattern in the sinuous-meandering reach and a delta characterized by the typical fractal structure Figure 3). The planform evolution and the continuous abandonment and activation of channels in the upstream sections of the study area were the result of a natural river flow that, during floods, was able to erode banks and deposit sediments over the river banks or along the channel where flow velocity locally decreased or secondary currents generated. This promoted channel bifurcations and allowed the deposition of mouth bars that, in turn, triggered channel avulsion generating the delta structure. Figure 5a,b and e showed that the increase in the area covered by bare sediments (Figure 5b) occurred after large rain events that increased the portion of wet study area (see Figure 5a, and e). This suggested that the rise in the portion of dry land covered by bare sediments was due to water retreating after floods and new sediments deposited during the flood that locally modified the floodplain topography.

Sediment deposition generated mouth bars and bifurcated the main channel, or in the case that a bifurcation already existed, it backfilled the channel and generated avulsion upstream, widening the bifurcation. However, this cyclic process is also controlled by the downstream boundary condition imposed by the lake level. It should be noted how after the highest level experienced by the lake within the investigated time frame, the Omo River presented almost half of the bifurcations observed in the channel in 1998 (see Figure 10). The number of channels remained low in the following years and the water coverage presented an increasing trend. In 2001 the number of distributary channels or bifurcations observed were very low due to the high level of the lake that did not allow the channels to be seen from satellite imagery. During the following five years, the number of bifurcations had progressively increased reaching a value of 10 as before the lake rose flooding the floodplain. Then, in one year, the channel bifurcations observed dropped to 5. After this, the river started to oscillate between 3 and 6 bifurcations. This diminished number of bifurcations was probably caused by the increase in the lake level that hampered the delta formation mechanism (Wang et al., 2019).

After the works to build the dam started, we observed a further decrease in the number of channels, with the delta morphology limited to one major bifurcation after 2012. It is reasonable to assume that this abrupt change in river morphodynamics is due to the reduced sediment load available for the river downstream the Gibe III dam. In particular, the impact of the lack of sediments for the river was threefold. First, to limit the deposition of mouth-bar and the channel backfilling mechanisms at the base of the formation of deltas. Second, to increase the erosion of the channel bed, which in turn reduces channel avulsion, and progressively disconnect the channel from its floodplain. Third, to reduce the average delta elevation via sediment erosion, further enhancing the effect associated to lake level rising discussed above. This latter phenomena is supported by the evolution of bare sediments coverage (Figure 3b). This is also evident from the autocorrelation function computed for

the bare ground signal before and after the dam was built (7b). The function showed that the autocorrelation time halved from 16 to 8 months, reaching a frequency close to that of the water coverage (7a). This means that, after the dam, the possibility to see dry or wet sediments from the image was directly associated to the water coverage. Such that sediments were exposed and visible during low river flow and low lake level, and submerged during and after floods or high lake levels.

It is possible that, before the works for the dam, the complex morphological structures and river morphology that characterized the study area provided preferential way for the overflow from either lake and river keeping large amounts of sediments exposed regardless the water depth. Finally, different temporal scales of the bare ground signal (Figure 7b) could be associated to the fact that in a more natural system, i.e. before the dam, more floods were required to rework the floodplain and the channel itself changing the sediment deposition pattern. This concept is, however, directly influenced by vegetation dynamics, since plants are able to increase the resistance to sediment erosion. In order to remove a vegetated sediment deposit, the magnitude of the flood needs to be larger than the one that generated the deposit, of a quantity which is proportional to the plant stage of development (Corenblit et al., 2007).

5.3 Vegetation dynamics and interaction with river and lake processes

The analysis revealed that changes in vegetation distribution have accompanied the heavy morphological evolution of the river. The autocorrelation function computed for both dense and sparse vegetation biomass presented the same frequency of water before the dam was built. This means that, during floods either or both river and lake side vegetation were killed, removed or damaged. Evidence of this can be appreciated in the historical signal of Figure 5c and d, where rain events (Figure 5e) or increases in water coverage (Figure 5a) are associated to a decrease in vegetation biomass. This variation is more evident in sparse vegetation biomass than for dense vegetation biomass. We could explain this behaviour by recalling that plant clusters provide self-protection to plants by reducing the drag and channel bed erosion (Nepf, 2012). Single stands growing at the top of the river banks or shrubs populating the mudflood (Carr, 1998) would be easily uprooted during floods, experience anoxic conditions related to high water depth or because they are buried by sediments. After the dam was built, the signal associated to sparse vegetation biomass increased the correlation on almost 6 months. Dense vegetation reduced its autocorrelation on few months but after that, the function remained null for almost a year, meaning that part of the recent signal showed no correlation, i.e. white noise. Changes in vegetation coverage associated to the disturbance generated by the dam will require longer time scales, will affect also sparse vegetation, and will not show a random pattern. Therefore, it is possible that the random changes in dense vegetation biomass observed were caused by small fires lightened by local people to free some space for cattle activities.

We investigated the impact that changes in local temperature and water level could have had on the vegetation. We showed that higher air temperature (Figure 6a) did not affect vegetation dynamics since no major changes were observed in the cross-correlation functions (Figure 8c and d). It is interesting to notice though that air temperature is anticorrelated with sparse vegetation biomass compared with dense vegetation biomass. This can be associated with a higher stress provided to isolated stand or shrubs by an increase in temperature, particularly in arid or semi-arid environments, compared to dense vegetation biomass that can mitigate the effect of temperature on the evapotranspiration rate.

More interesting are the cross-correlation functions obtained for the two type of vegetation biomass and changes in wet surface (i.e. bare ground plus water). The signals are obviously anticorrelated and show a major change in their time scales before and after the dam was built. Both sparse and dense vegetation reduced the time lag for which they

are correlated with the variation of sediments and water by almost half (Figure 8a and b). In addition, since 2016 the dam controls the river flow that present two peaks per year, compared to the only peak experienced during the flood season per year. This may have influenced the signal, although it had an impact on a limited portion of it. The reduced time in which vegetation becomes correlated with water variations means that the higher and almost constant low flow provides a more suitable environment for plants (e.g. higher and constant water table) that grow faster. Field observations associated the low presence of plants along the river with the high seasonal fluctuations of soil moisture. After the dam, the controlled flow shortened the flood season and reduced floods magnitude by limiting the possibility of flood to remove vegetation via uprooting or anoxic conditions. Plants are even more protected by a probably incised channel that further reduces the chances of overflow. The fact that less plants are removed or die during floods is also supported by the lack of bare sediments observed in Figure 5b.

As a results, the vegetation biomass distribution has changed, which is evident from the temporal evolution of the statistics computed for the NDVI distribution (Figure 9). The values, particularly the kurtosis, revealed that after the dam was built the local vegetation tends to present more dense biomass (high values of NDVI) compared to the scenario before the dam where vegetation biomass appeared well distributed between sparse and dense. It is however unclear weather existing vegetation types are more diffused due to changes in river and floodplain morphodynamics or new alien species have colonized the study area along with the existing ones. To the best of our knowledge, no studies have been conducted with the detail of the investigation performed by (Carr, 1998), which could shed light on this evolution in the vegetation coverage.

Finally, a remark should be added on the use of the NDVI in this work, since NDVI depends on the time of the year the image was taken, e.g. plant vegetative state. Because of this, the comparison between two different dates may lead to misinterpretations on the evolution of vegetation within the study area. In order to get rid of this uncertainty, in our analysis we referred to the long term trend by investigating the time signals for vegetation coverage and the long term evolution of the statistics of the NDVI distribution within the study area. Figure 11 shows a schematic of the different probability distribution of the NDVI values for the study area that characterizes the time period before and after the dam.

5.4 Conceptual scheme and future evolution of the study area

Results have showed that the Omo River planform and the surrounding area has heavily changed during the last decades. Reasons for this can be found in the variation of the lake level, a modified river hydrology, and a diminished sediment load. We discussed above how these changes may have impacted the land coverage of the study area and river morphodynamics. The main result is that the Omo River became less dynamic with time, abandoning secondary/distributary channels and possibly deepening its channel bed, and vegetation biomass growth in density. Studies on delta formations have shown that deltas characterized by deep channels require larger disturbance to be modified (M. Van Dijk et al., 2012), and their evolutionary time scales increase proportionally to the length of the channel and sediment load reduction.

It is therefore reasonable to think that the lower reach of the Omo River and the delta region have reached a new stable equilibrium state with less variations than the previous one. In the past, the Omo River was highly dynamic and able to rework its morphology periodically. While during floods, the deposition of fluvial bar modified the flow pattern inducing channel avulsion and bifurcations. This generated new channels or widened existing ones that eventually were abandoned during the subsequent dry season. In order to restore the previous state of the system, massive changes are required about the boundary conditions imposed upstream by the dam, i.e. sediment load and water flow, downstream by the lake level. This will change the channel slope and depth and reactivate that cyclic

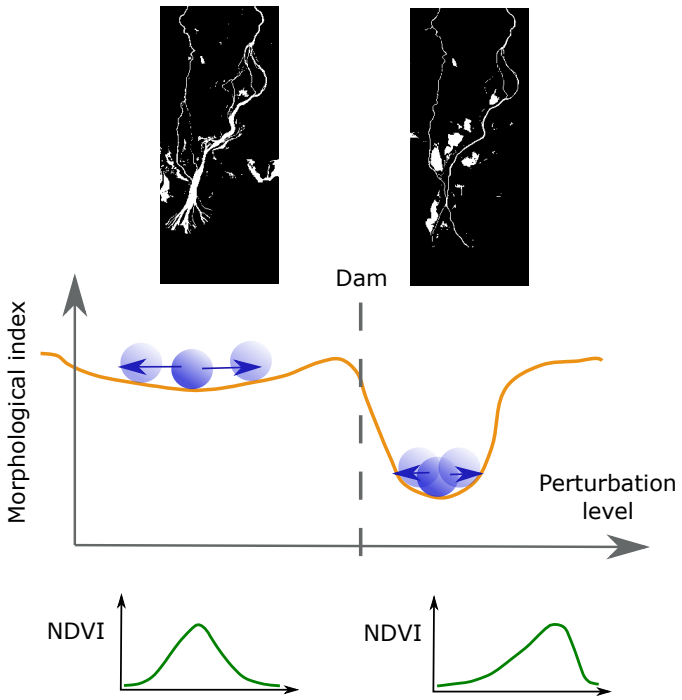

Figure 11. Conceptual model of the changes in eco-morphological processes observed for the lower reach of the Omo River.

process of mouth bar deposit and avulsion at the base of delta formation. Consequentially, the population of plants will change further promoting the establishment of a dynamic ecosystem.

Changes in climate variables should also be taken into account when considering if the river system could return to the previous, more dynamic, configuration. A recent modelling study exploring the next 20 years suggested that climate change will modify precipitation patterns increasing the magnitude and frequency of floods, and thus the overall lake inflow (UNEP-DHI-Centre, 2021). The lake level will therefore keep rising since it is unlikely that the increase in temperature observed (Figure 6a) may affect the evaporation rate such that to contrast the positive trend of the flow rate induced by more frequent rain events. On the other hand, the increasing need of water for crops irrigation within the Omo basin could affect this trend and progressively reduce the water level of the lake. The rapid expansion of cotton crops within the last years have increased the amount of water flow subtracted to the Omo River downstream the dam, reducing almost by half the base inflow of the Turkana Lake. This scenario will be further exacerbated by the application of the future cultivation plans already approved for 2025 which will further diminish the water flow of the Omo to a quarter of that initially released by the dam, and the construction of two other dams, the Gibe IV and Gibe V downstream the Gibe III. As a result, the lake level will drop with serious consequences for the fish communities particularly those close to the shores (especially during breeding season). The low water table will change the vegetation type as well as its spatial distribution, and floods will not be able to modify channel morphology. So far, studies on future trajectories have been investigating mostly lake level variations, but future research should focus also on vegetation and channel dynamics. Such studies will

help to identify management actions that could help to restore previous processes of the Omo river and bring the ecosystem to a new equilibrium.

References

Acharya, T. D., Subedi, A., & Lee, D. H. (2018). Evaluation of water indices for surface water extraction in a landsat 8 scene of nepal. *Sensors*, *18*(8), 2580.

Amri, R., Zribi, M., Lili-Chabaane, Z., Duchemin, B., Gruhier, C., & Chehbouni, A. (2011). Analysis of vegetation behavior in a north african semi-arid region, using spot-vegetation ndvi data. *Remote sensing*, *3*(12), 2568–2590.

Avery, S. (2011). Hydrological impacts of ethiopia's omo basin on kenya's lake turkana. *presented under "Global Programs and Strategies on Assessment and Management of Lakes and Their Basins: UNEP/ILEC Collaboration", 14th World Lake Conference, Austin, Texas, USA, 3rd November 2011*.

Avery, S. (2012). Lake turkana & the lower omo: hydrological impacts of major dam and irrigation developments. *African Studies Centre, the University of Oxford*.

Ayalew, L. (2009). Analyzing the effects of historical and recent floods on channel pattern and the environment in the lower omo basin of ethiopia using satellite images and gis. *Environmental geology*, *58*(8), 1713–1726.

Bau', V., Zen, S., Calvani, G., & Perona, P. (2019). Extracting the critical rooting length in plant uprooting by flow from pullout experiments. *Water Resources Research*, *55*(12), 10424–10442.

Calvani, G., Perona, P., Zen, S., Solari, L., et al. (2019). Return period of vegetation uprooting by flow. *Journal of Hydrology*, *578*, 124103.

Camporeale, C., Perucca, E., Ridolfi, L., & Gurnell, A. (2013). Modeling the interactions between river morphodynamics and riparian vegetation. *Reviews of Geophysics*, *51*(3), 379–414.

Caponi, F., & Siviglia, A. (2018). Numerical modeling of plant root controls on gravel bed river morphodynamics. *Geophysical Research Letters*, *45*(17), 9013–9023.

Carr, C. J. (1998). Patterns of vegetation along the omo river in southwest ethiopia. *Plant Ecology*, *135*(2), 135–163.

Corenblit, D., Tabacchi, E., Steiger, J., & Gurnell, A. M. (2007). Reciprocal interactions and adjustments between fluvial landforms and vegetation dynamics in river corridors: a review of complementary approaches. *Earth-Science Reviews*, *84*(1-2), 56–86.

ECMWF. (2021). `https://www.ecmwf.int/`. (Accessed: 2021-08-17)

Edmonds, D., & Slingerland, R. (2007). Mechanics of river mouth bar formation: Implications for the morphodynamics of delta distributary networks. *Journal of Geophysical Research: Earth Surface*, *112*(F2).

Feyisa, G. L., Meilby, H., Fensholt, R., & Proud, S. R. (2014). Automated water extraction index: A new technique for surface water mapping using landsat imagery. *Remote Sensing of Environment*, *140*, 23–35.

Głogowski, A., Perona, P., Bryś, K., & Bryś, T. (2021). Nonlinear reconstruction of bioclimatic outdoor-environment dynamics for the lower silesia region (sw poland). *International Journal of Biometeorology*, 1–15.

Gorelick, N., Hancher, M., Dixon, M., Ilyushchenko, S., Thau, D., & Moore, R. (2017). Google earth engine: Planetary-scale geospatial analysis for everyone. *Remote Sensing of Environment*. Retrieved from `https://doi.org/10.1016/j.rse.2017.06.031` doi: 10.1016/j.rse.2017.06.031

Gurnell, A. (2014). Plants as river system engineers. *Earth Surface Processes and Landforms*, *39*(1), 4–25.

Haack, B. (1996). Monitoring wetland changes with remote sensing: an east african example. *Environmental Management*, *20*(3), 411–419.

Henshaw, A. J., Gurnell, A. M., Bertoldi, W., & Drake, N. A. (2013). An assessment of the degree to which landsat tm data can support the assessment of fluvial dynamics,

as revealed by changes in vegetation extent and channel position, along a large river. *Geomorphology*, *202*, 74–85.

Kim, W., & Jerolmack, D. J. (2008). The pulse of calm fan deltas. *The Journal of Geology*, *116*(4), 315–330.

Muñoz Sabater, J. (2019). Era5-land monthly averaged data from 1981 to present. *Copernicus Climate Change Service (C3S) Climate Data Store (CDS).(Accessed: 2021-08-17), doi:10.24381/cds.68d2bb30*.

Nepf, H. M. (2012). Hydrodynamics of vegetated channels. *Journal of Hydraulic Research*, *50*(3), 262–279.

Nittrouer, J. A., Shaw, J., Lamb, M. P., & Mohrig, D. (2012). Spatial and temporal trends for water-flow velocity and bed-material sediment transport in the lower mississippi river. *Bulletin*, *124*(3-4), 400–414.

Piliouras, A., & Kim, W. (2019). Delta size and plant patchiness as controls on channel network organization in experimental deltas. *Earth Surface Processes and Landforms*, *44*(1), 259–272.

Politti, E., Bertoldi, W., Gurnell, A., & Henshaw, A. (2018). Feedbacks between the riparian salicaceae and hydrogeomorphic processes: A quantitative review. *Earth-Science Reviews*, *176*, 147–165.

Reitz, M. D., Jerolmack, D. J., & Swenson, J. B. (2010). Flooding and flow path selection on alluvial fans and deltas. *Geophysical Research Letters*, *37*(6).

Rouse, J. W., Haas, R. H., Schell, J. A., Deering, D. W., & Harlan, J. C. (1974). Monitoring the vernal advancement and retrogradation (green wave effect) of natural vegetation. *NASA/GSFC Type III Final Report, Greenbelt, Md*, *371*.

Tian, F., Brandt, M., Liu, Y. Y., Verger, A., Tagesson, T., Diouf, A. A., ... Fensholt, R. (2016). Remote sensing of vegetation dynamics in drylands: Evaluating vegetation optical depth (vod) using avhrr ndvi and in situ green biomass data over west african sahel. *Remote Sensing of Environment*, *177*, 265–276.

Tron, S., Perona, P., Gorla, L., Schwarz, M., Laio, F., & Ridolfi, L. (2015). The signature of randomness in riparian plant root distributions. *Geophysical Research Letters*, *42*(17), 7098–7106.

UNEP-DHI-Centre. (2021). Support to sustainable development in lake turkana and its river basins. results of modelling of future scenarios of lake turkana and its river basins. (United Nations Environment Programme (UNEP), Technical Report)

USGS-Landsat7. (2021). `https://www.usgs.gov/core-science-systems/nli/landsat/landsat-7?qt-science_support_page_related_con=0#qt-science_support_page_related_con`. (Accessed: 2021-08-18)

Van Dijk, M., Kleinhans, M. G., Postma, G., & Kraal, E. (2012). Contrasting morphodynamics in alluvial fans and fan deltas: effect of the downstream boundary. *Sedimentology*, *59*(7), 2125–2145.

Van Dijk, W., Teske, R., Van de Lageweg, W., & Kleinhans, M. (2013). Effects of vegetation distribution on experimental river channel dynamics. *Water Resources Research*, *49*(11), 7558–7574.

Wang, J., Muto, T., Urata, K., Sato, T., & Naruse, H. (2019). Morphodynamics of river deltas in response to different basin water depths: An experimental examination of the grade index model. *Geophysical Research Letters*, *46*(10), 5265–5273.

Zaniolo, M., Giuliani, M., Sinclair, S., Burlando, P., & Castelletti, A. (2021). When timing matters—misdesigned dam filling impacts hydropower sustainability. *Nature Communications*, *12*.

Zen, S., & Perona, P. (2020). Biomorphodynamics of river banks in vegetated channels with self-formed width. *Advances in Water Resources*, *135*, 103488.

Zen, S., Zolezzi, G., Toffolon, M., & Gurnell, A. M. (2016). Biomorphodynamic modelling of inner bank advance in migrating meander bends. *Advances in Water Resources*, *93*, 166–181.